Journal of Molecular Graphics and Modelling 51 (2014) 184–192

Contents lists available at ScienceDirect

Journal of Molecular Graphics and Modelling

journal homepage: www.elsevier.com/locate/JMGM

Nonadiabatic reaction mechanisms of the O(^{3}P) with cyclopentene

Hongmei Zhao, Kunhui Liu, Di Song, Hongmei Su*

State Key Laboratory of Molecular Reaction Dynamics, Beijing National Laboratory for Molecular Sciences (BNLMS), Institute of Chemistry, Chinese Academy of Sciences, Beijing 100190, China

ARTICLE INFO

Article history:
Accepted 23 May 2014
Available online 2 June 2014

Keywords:
Cyclopentene
Oxygen
Nonadiabatic pathway
Minimum energy crossing points
Enol

ABSTRACT

The reaction mechanism of the ground state oxygen atom O(^{3}P) with cyclopentene is investigated theoretically. The triplet and singlet potential energy surfaces are calculated at the CCSD(T)//MP2/6-311G(d,p) level and the minimum energy crossing points (MECPs) between the two surfaces are located by means of the Newton–Lagrange method, from which the complex nonadiabatic reaction pathways are revealed. Based on the theoretical results, the most probable reaction mechanism of O(^{3}P) with c-C_5H_8 is described, which agrees with the experimental results nicely, including the condensed phase experiment. At the same time, the newly revealed reaction mechanism clarifies the previous controversial product distribution, and predicts the possible existence of the new enol product, cyclopentenol.

1. Introduction

The reaction of the oxygen atom O(^{3}P) with alkenes is an attractive subject due to their importance in atmospheric chemistry [1]. It is also an important elementary reaction in understanding combustion chemistry and oxidation mechanisms of hydrocarbon [2–7]. Although the concentration of oxygen atom O(^{3}P) is low and cannot be compared with that of oxygen molecules, the rate coefficient of some reactions of O(^{3}P) and alkenes exceeds that of O_2 and alkenes by several orders of magnitude [8–10]. In the fuel-rich combustion of cyclopentene flames, the reaction of cyclopentene and oxygen atom proceeds rapidly with the rate coefficient of 1.27×10^{13} cm^3 mol^{-1} s^{-1} [11], which plays a very important role in studying the mechanisms for the combustion and oxidation of unsaturated hydrocarbon. On the other hand, the formation of epoxides from the addition of oxygen atom to the double bond represents an important reaction in synthetic chemistry.

The pioneering research about the reaction of O(^{3}P) with cyclopentene was carried out by Cvetanović et al. [12,13]. They found that the main reaction products were cyclopentenoxide (CPO), ethylene (C_2H_4), acrolein (Acr), and cyclopentanone (CPN) in the gas phase [13]. The major product was cyclopentenoxide (CPO). The minor formation of cyclobutylcarboxaldehyde (CBA), dihydropyran (DHP) and 4-pentenal (4-PA) was also observed in the experiment. In another condensed phase experiment [12] performed at low temperature of −196 °C, it was found that the fission to acrolein (Acr) and ethene (C_2H_4) was totally suppressed, while the product CBA was still observed. Due to the equal formation of ethylene (C_2H_4) and acrolein (Acr), it was postulated that these two products came from the direct fragmentation of one adduct. Based on the observed products, Cvetanović et al. [13] proposed the reaction mechanism shown in Scheme 1. According to this mechanism, the oxygen atom adds to the double bond of cyclopentene and yields the initial adduct, a "triplet diradical" intermediate (A), which reacts further through several pathways releasing various products. The cyclopentenoxide (CPO) and cyclopentanone (CPN) are generated from the rearrangement of the diradical intermediate (A) directly. The ring cleavage of diradical intermediate (A) forms an acyclic diradical (B). Subsequently, the acyclic diradical (B) can fragment into acrolein (Acr) and ethene (C_2H_4), rearrange to cyclobutylcarboxaldehyde (CBA), or lead to other minor products of 4-pentenal (4-PA) and dihydropyran (DHP).

Several years later, another group [14] also studied the reaction of c-C_5H_8 + O(^{3}P) in the gas phase and gave the controversial product distributions. The major product was cyclopentanone (CPN), but not cyclopentenoxide (CPO), the most major one found by Cvetanović and co-workers [13]. The minor products CBA and dihydropyran (DHP) identified by Cvetanović et al. [13] were not detected in their experiment.

In the present paper, the first theoretical study for the reaction of c-C_5H_8 + O(^{3}P) is provided to clarify the reaction mechanism and the product distribution. The reaction of O(^{3}P) with cyclopentene is initiated in the triplet state, but all the products observed are in the singlet state. Therefore, it is anticipated that crossing points between triplet and singlet states should play an important role in this reaction. The triplet and singlet potential energy surfaces

* Corresponding author. Tel.: +86 10 62562837; fax: +86 10 62563167.
E-mail address: hongmei@iccas.ac.cn (H. Su).

http://dx.doi.org/10.1016/j.jmgm.2014.05.008
1093-3263/

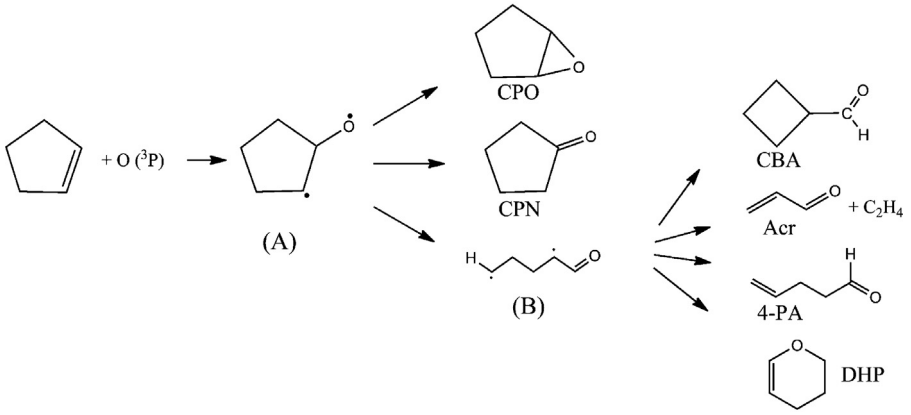

Scheme 1. Reaction mechanism proposed by Cvetanović et al. [13].

are calculated at the CCSD(T)//MP2/6-311G(d,p) level and the minimum energy crossing points (MECPs) between the two surfaces are located by means of the Newton–Lagrange method, from which the complex nonadiabatic reaction pathways are newly revealed. The most probable reaction mechanism of O(^{3}P) with c-C_5H_8 is described, which can rationalize the experimentally observed product distributions nicely. In addition, new product channels are predicted, which involves the formation of cyclopentenol, one kind of enols believed to be the key reaction intermediate in the hydrocarbon flames.

2. Computational methods

The equilibrium geometries of the reactants, products, various intermediates, and transition states are fully optimized using the restricted second-order Møller–Plesset perturbation (RMP2) method for the closed-shell system and the unrestricted second-order Møller–Plesset perturbation (UMP2) method for the open-shell system with the standard 6-311G(d,p) basis set. UMP2 energies obtained for the open-shell system are further corrected by running an unrestricted calculation which can project out the spin contamination from higher spin states (PMP2) [15]. The Frozen core (FC) approximation is used in all post-Hartree Fock calculation. Harmonic vibrational frequencies confirm that all the frequencies of the intermediates are real and the transition states have only one imaginary frequency. The zero-point energies (ZPE) are calculated at the same level based on the optimized geometries. The intrinsic reaction coordinate (IRC) [16] calculations are carried out to confirm the connections of the transition states between the right local minima. Further refined single-point energies are calculated by the coupled cluster CCSD(T) method [17]. Based on the Newton–Lagrange method, a homemade program is used to locate the minimum energy crossing point (MECP) on the intersection seam at the UMP2/6-311G(d,p) level. The Newton–Lagrange method was introduced by Koga and Morokuma [18] to find the crossing point where the energy is the lowest on the $(f-1)$-dimensional hypersurface of seam between two f-dimensional potential energy surfaces. We have applied this method successfully in locating the MECP for the reaction of O(^{3}P) with unsaturated hydrocarbons of alkenes and alkynes [19,20]. All of the calculations are performed with the Gaussian 03 program package [21].

3. Results and discussion

The optimized geometries of the reactants, intermediates, products and transition states in singlet and triplet states at the UMP2/6-311G* level are shown in Fig. 1. The single-point energies are further refined using CCSD(T) method based on the optimized structures. The obtained potential energy profiles in the triplet and singlet states are displayed in Figs. 2 and 3.

3.1. The minimum energy crossing points (MECPs) between the triplet and singlet states

Although the reaction of ground state oxygen and cyclopentene occurs initially in the triplet state, the main products were found to exist in the singlet state. Consequently, the reaction should occur nonadiabatically, crossing from the triplet state to the singlet state. In fact, multiple crossing points may exist between the triplet and singlet potential energy surfaces, among which the minimum energy crossing point (MECP) is the most important one along the nonadiabatic reaction pathways. The MECP is usually considered as a "transition state" between the two states and plays an important role in understanding the nonadiabatic reaction mechanism. The MECP can be located by the Newton–Lagrange method proposed by Koga and Morokuma [18]. The MECP has several main characteristics. First, MECP has the same structure and energy for the singlet and triplet states. Secondly, unlike the equilibrium or a transition state, the energy gradients of the MECP are not zero. Thirdly, the energy gradients of the MECP in the singlet state are proportional to that of the triplet state with the ratio of $-\lambda/(1-\lambda)$, where λ is the Lagrange multiplier. Using the Newton–Lagrange method, two MECPs, the MECP1 and MECP2, between the singlet and triplet state are located for the reaction of O(^{3}P) with c-C_5H_8.

3.2. Adiabatic pathways on the triplet potential energy surface

The potential energy profile of the adiabatic reaction channels on the triplet potential energy surface at the CCSD(T)//MP2/6-311G** level is shown in Fig. 2. There are two types of reaction in the triplet state: O-addition and H-abstraction.

3.2.1. The O-addition reaction

It can be seen from Fig. 2 that approaching of the triplet oxygen atom to the double bond of c-C_5H_8 leads to the formation of triplet adduct ^{3}IM1 via ^{3}TS1 by overcoming the energy barrier of 3.0 kcal mol^{-1}. There was the controversy about the structure of the initial adduct ^{3}IM1 in the O(^{3}P) addition to the double bond of olefins. Cvetanović et al. [12] postulated the triplet diradical intermediate as the initial adduct. Meanwhile, Scheer and Klein [22] proposed a nonclassical "transition state" with three-membered ring structure. According to our calculation, the addition of ground state oxygen atom occurs at one of the carbon atoms of the double bond, leading to the triplet diradical structure (^{3}IM1 shown in Fig. 1), which is in line with the postulation of Cvetanović et al. [12].

Starting from ^{3}IM1, there are four pathways (Shown in Fig. 2). The first MECP between triplet and singlet surface, MECP1 is only 0.2 kcal mol^{-1} above ^{3}IM1 in energy, suggesting that the intersystem crossing via MECP1 is energetically favorable. So the first pathway is the intersystem crossing via MECP1. The second pathway corresponds to a conformational rearrangement from the boat conformation ^{3}IM1 to the chair conformation ^{3}IM2 via ^{3}TS4 with a low barrier of 2.9 kcal mol^{-1}. Close to ^{3}IM2, the second MECP between triplet and singlet surface, MECP2, is located. It lies only 2.0 kcal mol^{-1} above ^{3}IM2 in energy, which is also expected to result in intersystem crossing. There is the third pathway, the ring opening reaction of ^{3}IM1 via ^{3}TS5 with a high barrier of 14.5 kcal mol^{-1}, leading to the triplet acyclic diradical (P1). The fourth pathway is the similar ring opening reaction of ^{3}IM2 leading

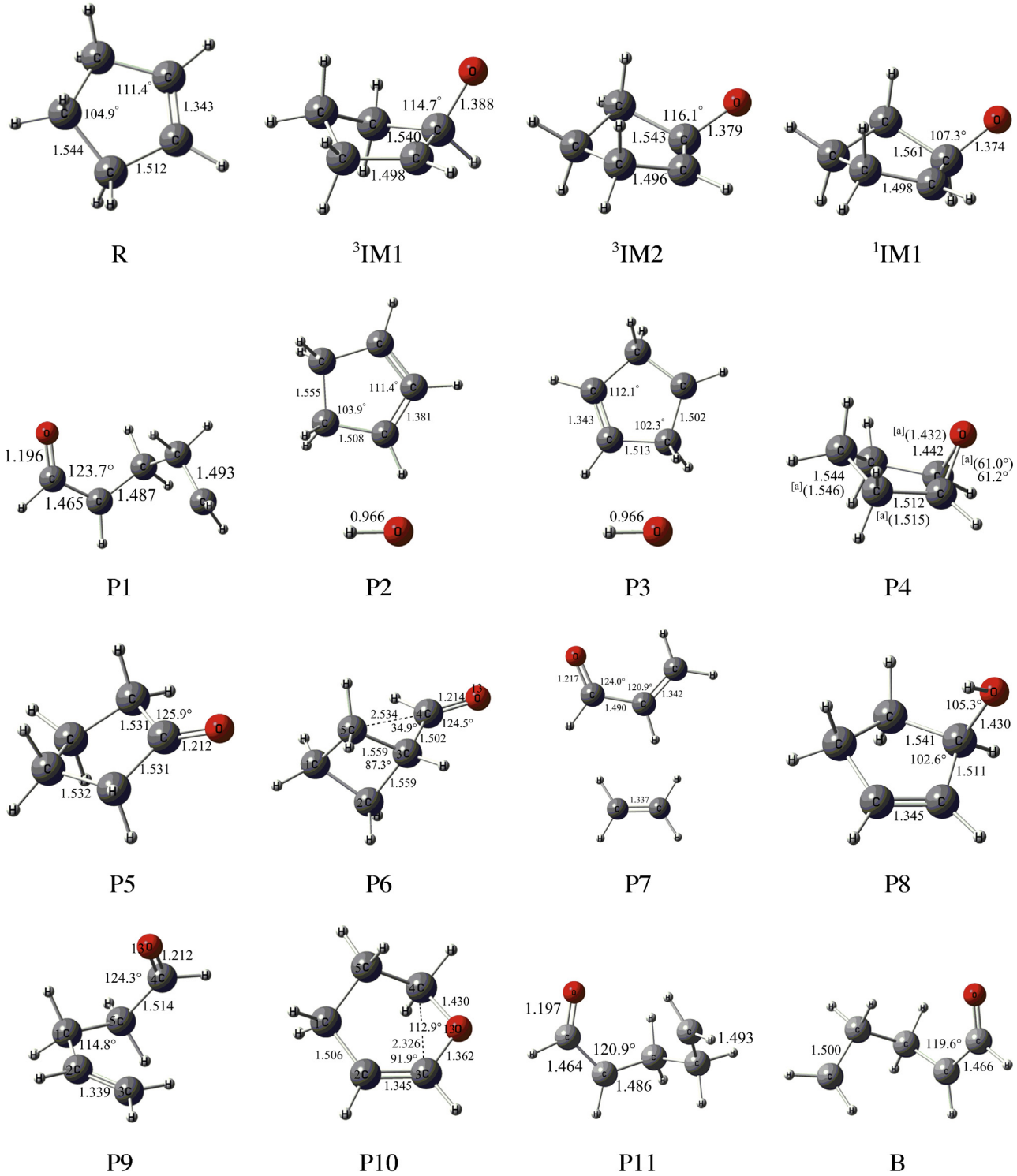

Fig. 1. The optimized geometries of reactants, intermediates, transition states, and products for the O(^{3}P) + c-C_5H_8 reaction at the MP2/6-311G(d,p) level. The minimum energy crossing points MECP1 and MECP2 are also shown. Bond lengths are in angstrom and bond angles are in degrees. For P4, structural parameters determined by experiments [25] are also included and labeled with superscript [a].

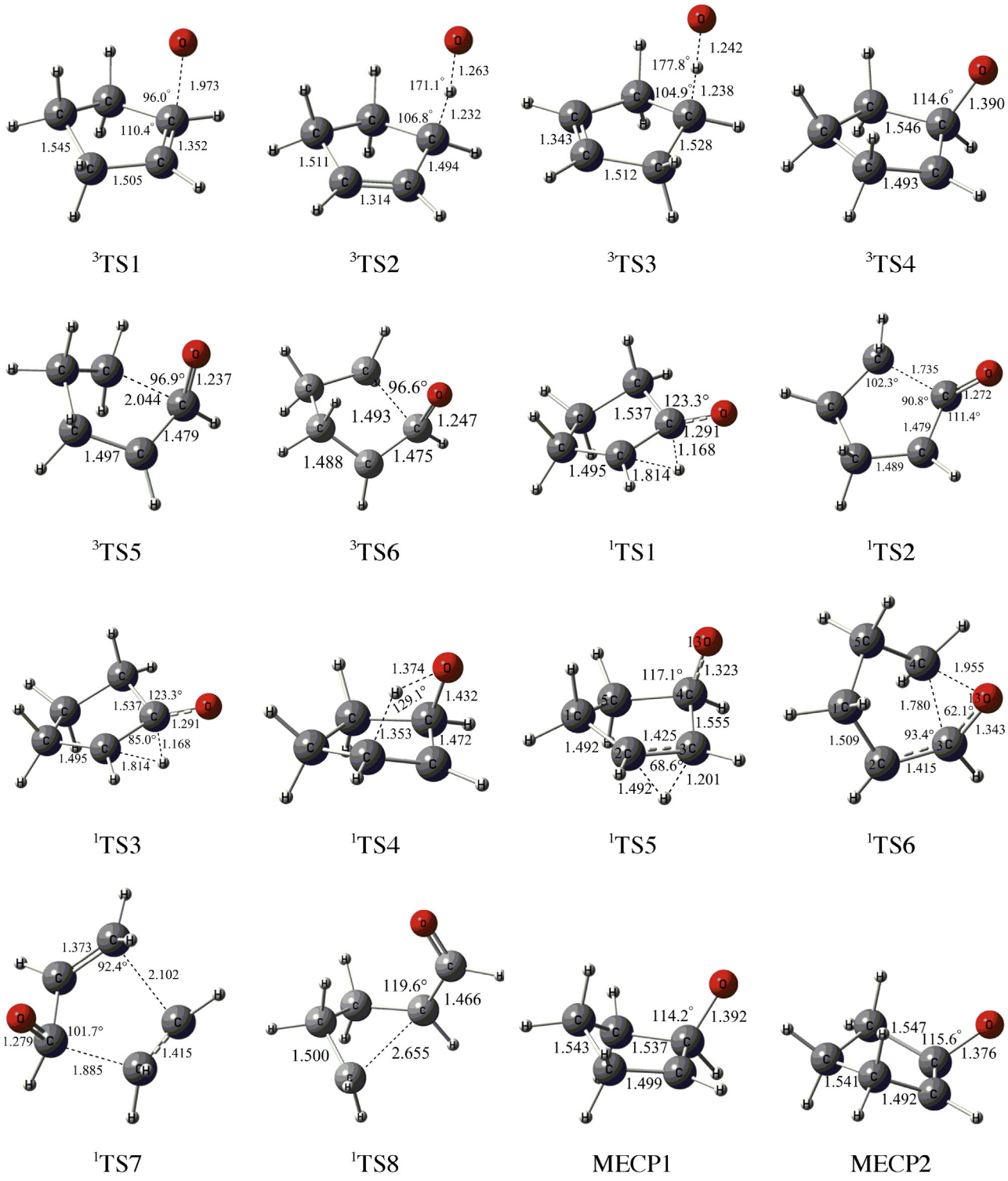

Fig. 1. (*Continued*).

to the formation of P11. The calculation showed that the further dissociation or rearrangement of P1 and P11 is energetically infeasible, and thus can be eliminated.

3.2.2. The H-abstraction reaction

In parallel to the O-addition, H-abstraction reaction may also take place in the triplet state. The oxygen atom abstracts one H atom from the carbon atom at ortho-position or meta-position of the double bond in cyclopentene by overcoming the energy barrier of 10.7 or 12.2 kcal mol^{-1} respectively. The barriers of H-abstraction reaction via ^{3}TS2 and ^{3}TS3 are 7.7 and 9.2 kcal mol^{-1} higher in energy than that of O-addition reaction via ^{3}TS1. Therefore the triplet reaction occurs dominantly via the O-addition rather than the H-abstraction mechanism. The product P2 and P3 of the H-abstraction reaction should contribute only as a small fraction of the total product.

Among all the pathways in the triplet state shown in Fig. 2, the intersystem crossing from triplet to singlet state via either MECP1

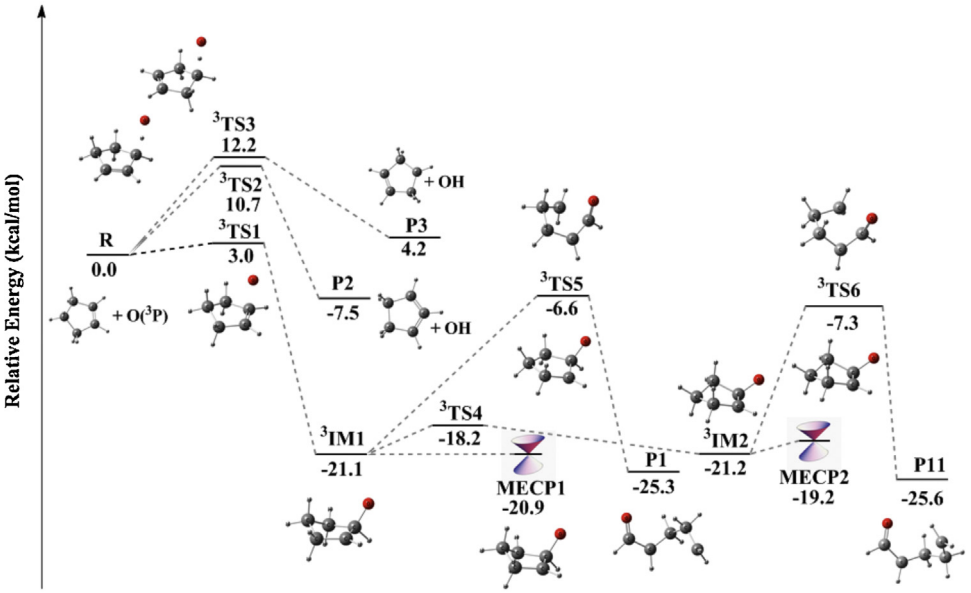

Fig. 2. Potential energy profiles of the adiabatic reaction pathways on the triplet surface obtained at the CCSD(T)//MP2/6-311G(d,p) level. All energies given are relative to the reactant. Carbon, oxygen, and hydrogen atoms are denoted with gray, red, and white balls respectively. (For interpretation of the references to color in this figure legend, the reader is referred to the web version of this article.)

or MECP2 corresponds to the lowest energy barriers and thus is the most energetically favorable. The reaction can cross to the singlet state and the singlet products will be yielded. It shows here that MECPs play key roles resulting in the nonadiabatic reaction pathways.

3.3. Nonadiabatic pathways on the singlet potential energy surface

Through the two crossing points, MECP1 and MECP2, a variety of nonadiabatic reaction pathways are open and the potential energy profiles are shown in Fig. 3. Pathways initiated from MECP1 and MECP2 are discussed separately in the following.

3.3.1. The pathways following MECP1

As shown in Fig. 3, the initial triplet adduct ^{3}IM1 crosses to the singlet state via MECP1 and rearranges simultaneously to cyclopentenoxide (CPO) by ring closure. The product CPO is labeled as P4 in the potential energy profile. The whole process forming CPO is nearly barrierless.

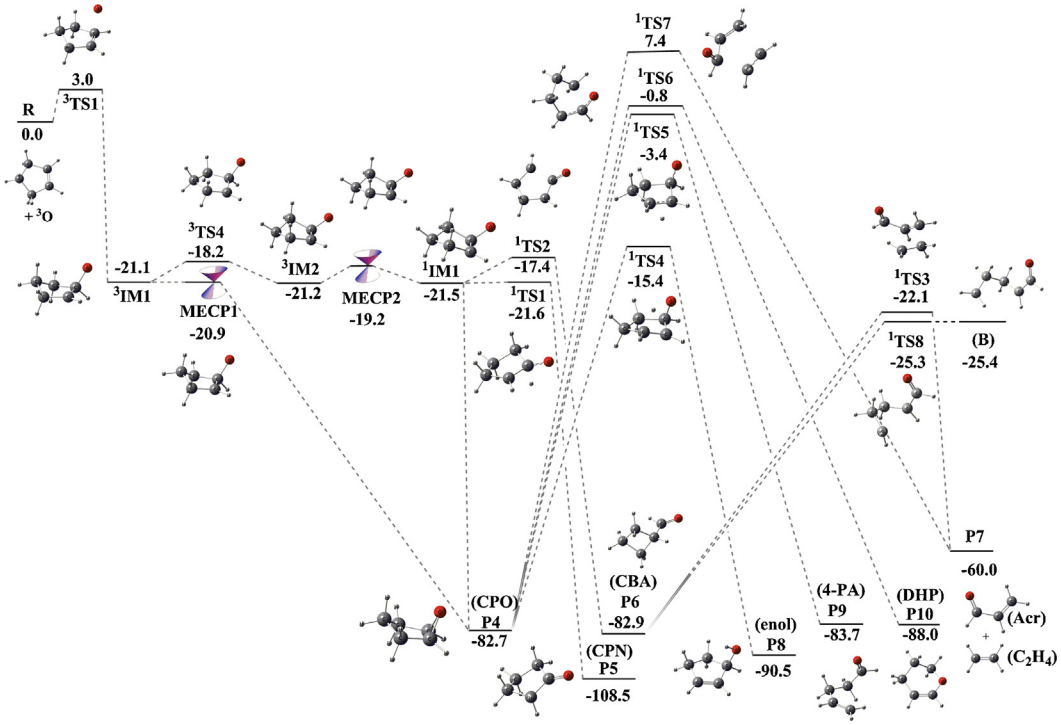

Fig. 3. Potential energy profiles of the nonadiabatic reaction pathways obtained at the CCSD(T)//MP2/6-311G(d,p) level. All energies given are relative to the reactant. Carbon, oxygen, and hydrogen atoms are denoted with gray, red, and white balls respectively. (For interpretation of the references to color in this figure legend, the reader is referred to the web version of this article.)

As an important product, the structure of cyclopentenoxide (CPO) has been determined experimentally [24], which can be compared with the currently calculated structures. From our calculation, the most stable structure of cyclopentenoxide (CPO) is found to exist with the boat conformation, but not the chair conformation, as shown in Fig. 1 (labeled as P4). This agrees with the microwave spectrum experimental results [23] that the cyclopentenoxide had the boat conformation in its ground vibrational state. The structure parameters of cyclopentenoxide (CPO) have been determined experimentally [24] based on the rotational constants for all isotopomers using the Kraitchman's equations [25], which are labeled with [a] in Fig. 1. Our calculated results at the MP2/6-311G(d,p) level are also shown in Fig. 1. It can be seen that the calculated structure agrees well with the experimentally determined parameters, demonstrating that the current MP2/6-311G(d,p) level of calculation can provide reliable information for the reaction of $O(^3P)$ with cyclopentene.

Starting from P4 (the cyclopentenoxide CPO), there are four pathways to form other products. (i) The isomerization of P4 leads to 2-cyclopentenol (P8) via a direct hydrogen migration transition state ^{1}TS4, whose energy is lying 15.4 kcal mol^{-1} below the reactant. (ii) P4 converts to P9, 4-pentenal (4-PA) via ^{1}TS5 lying 3.4 kcal mol^{-1} below the reactant. (iii) P4 can also rearrange to another minor product P10, the six-membered ring dihydropyran (DHP) via ^{1}TS6 lying 0.8 kcal mol^{-1} below the reactant. (iv) The decomposition of P4 leads to ethylene + acrolein (P7), via ^{1}TS7 lying 7.4 kcal mol^{-1} above the reactant.

Along the nonadiabatic pathways following MECP1, the cyclopentenoxide P4 is the first stable product, with a relative energy of 82.7 kcal mol^{-1} compared to reactant. The formation of P4 via MECP1 is barrierless, suggesting its favorable formation as a major product. Subsequently, the energized product P4 without being deactivated can undergo further decomposition or rearrangement, leading to four other secondary products (P7–P10), among which the formation of 2-cyclopentenol (P8) channel is energetically more favorable than the other three. Although the subsequent reaction pathways of P4 requires surmounting high barriers, the transition states locate either below the reactant or only 7.4 kcal mol^{-1} above the reactant. This means that these secondary product channels (P7–P10) are still energetically accessible, but their product distributions are certainly less than that of the primary major product P4, the cyclopentenoxide (CPO).

3.3.2. The pathways following MECP2

The second triplet and singlet crossing point, MECP2, locates only 2.0 kcal mol^{-1} above the triplet adduct ^{3}IM2, through which an intersystem crossing occurs and the singlet adduct ^{1}IM1 is formed (See Fig. 3). From ^{1}IM1, three pathways are located, yielding P4 (CPO), P5 (CPN) and P6 (CBA) respectively. The most favorable channel is the formation of P4, the cyclopentenoxide (CPO), through a barrierless ring closure of ^{1}IM1. In competition with this channel, the other two channels are described separately in the following.

3.3.2.1. The formation of cyclopentanone (P5). Another channel starting from ^{1}IM1 is the formation of P5, the cyclopentanone (CPN), through a direct hydrogen shift transition state (^{1}TS1), which has a three-membered ring structure. ^{1}TS1 is isoenergetic to ^{1}IM1, indicating that the formation of P5 is barrierless and should occur favorably. The H connected with carbon atom of C—O bond is transferred to the adjacent carbon and the C—O bond length is reduced from 1.374 Å in ^{1}IM1 to 1.291 Å in ^{1}TS1. Then a carbonyl (C═O) bond (1.212 Å) is formed, corresponding to the formation of cyclopentanone (CPN). CPN falls around the global minimum of the potential energy surface (108.5 kcal mol^{-1} below the initial reactants) and represents the most stable product.

3.3.2.2. The formation of cyclobutylcarboxaldehyde CBA (P6). The third channel starting from ^{1}IM1 is the formation of P6, Cyclobutylcarboxaldehyde (CBA), via the ring opening transition state ^{1}TS2. ^{1}TS2 has only one imaginary frequency of 525.2i and the direction of vibration vector along the breaking C—C bond indicates that ^{1}TS2 is the ring opening transition state. ^{1}TS2 is 4.1 kcal mol^{-1} above ^{1}IM1, which means that a low barrier of 4.1 kcal mol^{-1} is required for the formation of CBA. The product distribution of CBA is thus anticipated to be less than that of CPO and CPN that are all formed without barrier. But ^{1}TS2 is still 17.4 kcal mol^{-1} below the initial reactants and can be easily surmount by the available energy of the reactants. So the formation of CBA should still be a facile process.

According to the reaction mechanism proposed by Cvetanović et al. [13] (See Scheme 1), the cyclic diradical adduct (A), labeled as ^{1}IM1 in Fig. 3, will convert to an acyclic diradical C$^\bullet$H$_2$CH$_2$CH$_2$C$^\bullet$HCHO (B) by a ring opening reaction. Whereas it shows here in our calculation that the ring opening reaction of the cyclic diradical adduct will lead to the four-membered ring product CBA, instead of the acyclic diradical C$^\bullet$H$_2$CH$_2$CH$_2$C$^\bullet$HCHO.

In order to confirm that the ring opening reaction of the cyclic diradical adduct leads to the formation of CBA directly, we performed careful intrinsic reaction coordinate (IRC) calculations and analyzed the spin density evolution along the reaction coordinate. As shown in Fig. 4(a), IRC calculations demonstrate that ^{1}TS2 leads to the four-membered ring CBA (P6), but not the acyclic diradical C$^\bullet$H$_2$CH$_2$CH$_2$C$^\bullet$HCHO (B). What is the reason that CBA is formed instead of acyclic diradical (B)? To reveal the reaction process in detail, the spin densities of some representative IRC points are monitored and the results are shown in Fig. 4(b).

The ring-opening process of the singlet diradical ^{1}IM1 can be investigated by tracing atomic spin densities during the reaction. The spin densities of representative IRC points (^{1}TS2, IRC1, IRC2 and IRC3) are calculated using MP2 method, which is a reliable method to obtain meaningful spin density distributions for such diradical systems. The spin density distribution plots are illustrated as surface maps in Fig. 4(b). The blue regions indicate the accumulation of α spin density and the regions shown in red denote the β spin density distribution.

Based on the spin densities of ^{1}TS2, IRC1, IRC2 and IRC3, the ring-opening process can be described. Starting from ^{1}TS2, the homolytic 4C–5C bond cleavage occurs and unpaired α and β electrons are localized on 4C and 5C, respectively. The single α electron of 4C will be easily paired with the single β electron of the adjacent oxygen atom 13O. Therefore, a 4C═13O double bond is formed in ^{1}TS2. After 4C–5C bond fission, another singlet diradical structure, with one single α electron localized on 3C and the other single β electron on 5C, has been obtained in IRC1 and IRC2. β spin density on 5C atom and α spin density on 3C of IRC1 and IRC2 have strong interaction, and the attraction between 5C and 3C force them to move closer, which leads to the formation of 3C–5C bond and the four-membered ring product CBA (P6) is yielded at last. These results demonstrate that the strong spin–spin interaction intrinsically leads to the formation of product CBA (P6) instead of the acyclic diradical (B). The formation of CBA can also be envisioned from bond length changes along the intrinsic reaction coordinate (IRC) shown in Fig. 4(c). It can be clearly seen that as the distance between 4C and 5C increases during the 4C–5C bond breaking, the distance between 3C and 5C decreases to form a new 3C–5C bond (1.559 Å) corresponding to the CBA (P6) formation.

Starting from CBA (P6), the acyclic diradical C$^\bullet$H$_2$CH$_2$CH$_2$C$^\bullet$HCHO (B), which is thought to be an important intermediate by Cvetanović et al. [13] is formed via ^{1}TS8. And the acyclic diradical (B) is 57.5 kcal mol^{-1} higher in energy than P6. The relative energies of ^{1}TS8 and B are very close. Therefore, the acyclic diradical (B) could also go back to form P6.

3.3.2.3. The formation of ethylene + acrolein (P7). As shown in Fig. 3, the energized product CBA (P6) can undergo subsequent decomposition, resulting in equal amount of ethylene (C_2H_4) with acrolein (Acr) (P7) via ^{1}TS4, which is 22.1 kcal mol^{-1} below the initial reactants. So the formation of ethylene + acrolein (P7) is also energetically accessible and should constitute an important product channel, which is consistent with the experimental results of Cvetanović et al. [13] and Hoyermann et al. [14]. In particular, our calculation can explain the condensed phase experimental results reasonably. It has been shown in the condensed phase experiment [12] that the products of ethylene + acrolein (P7) were not found while CBA (P6) was still observed at −196 °C. It can be seen from our calculation that the ethylene and acrolein (P7) could be produced by overcoming the barrier of 60.8 kcal mol^{-1} from the fission of CBA (P6). When the temperature is low, there is no enough energy available to overcome such a high barrier and the formation of ethylene + acrolein (P7) would then be greatly suppressed, although CBA (P6) can still be formed because its formation is nearly barrierless.

The decomposition of cyclopentenoxide (CPO) (P4) also leads to ethylene + acrolein (P7), via ^{1}TS7 with a barrier of 90.1 kcal mol^{-1}, which is 29.5 kcal mol^{-1} higher than that of the fission of CBA (P6) to ethylene + acrolein (P7). Therefore it is anticipated that most of the ethylene and acrolein (P7) should be resulted from the decomposition of CBA (P6), but not from cyclopentenoxide CPO (P4).

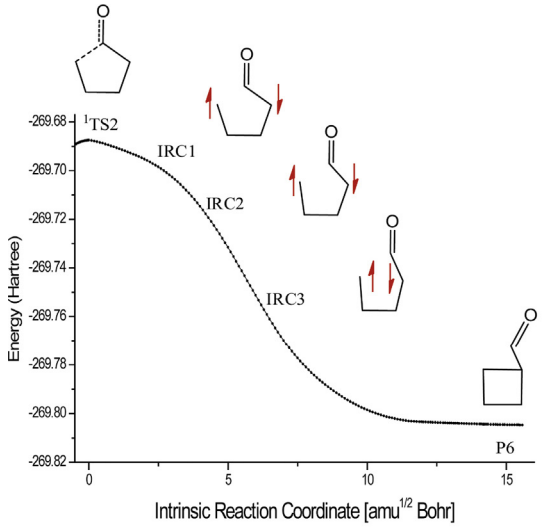

(a)

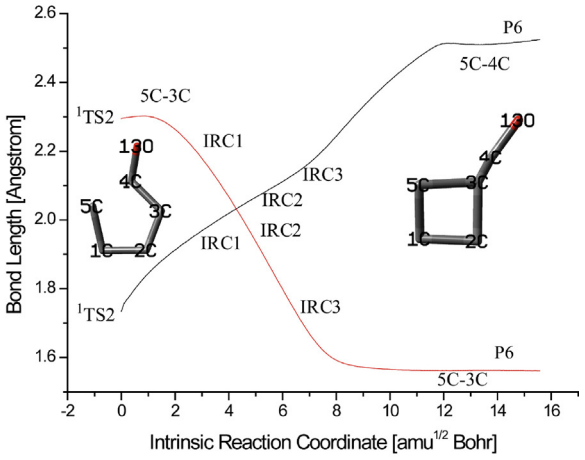

(b)

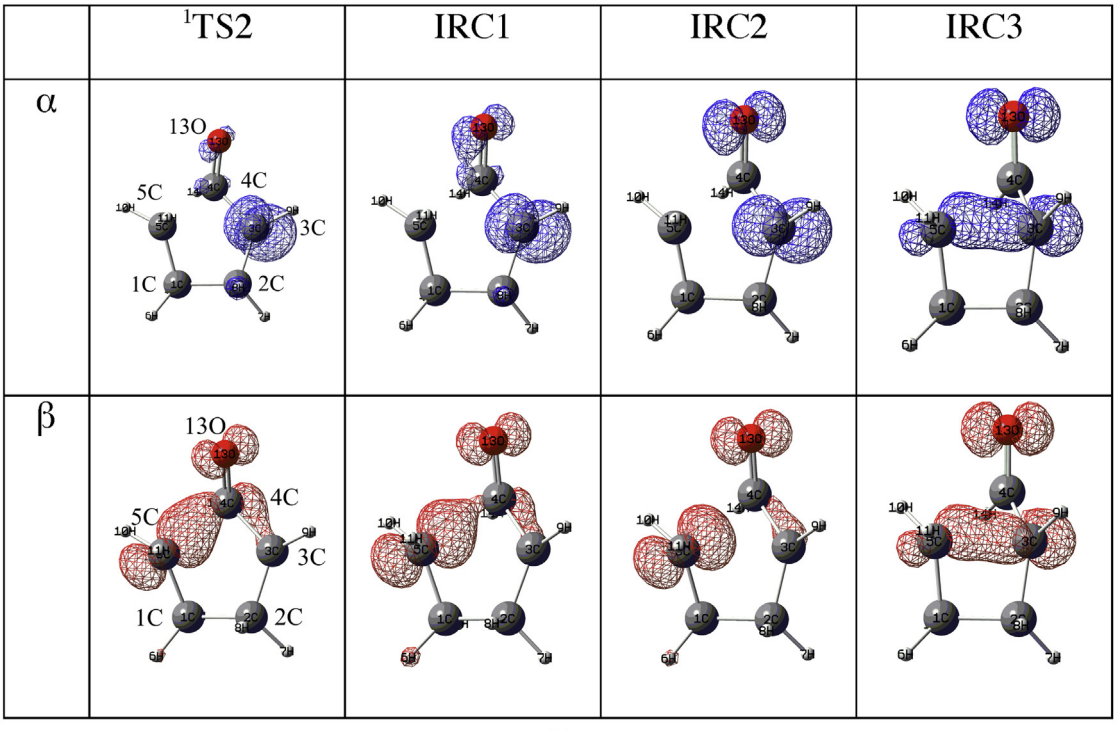

(c)

Fig. 4. (a) Energy profile along the intrinsic reaction coordinate (IRC) from transition state (^{1}TS2) to the product P6. (b) The mapped surface plots of α and β spin density distributions for the representative IRC points. The surface isovalue used is 0.01 a.u. (c) Changes of bond lengths along IRC during the formation of P6. (For interpretation of the references to color in the text, the reader is referred to the web version of this article.)

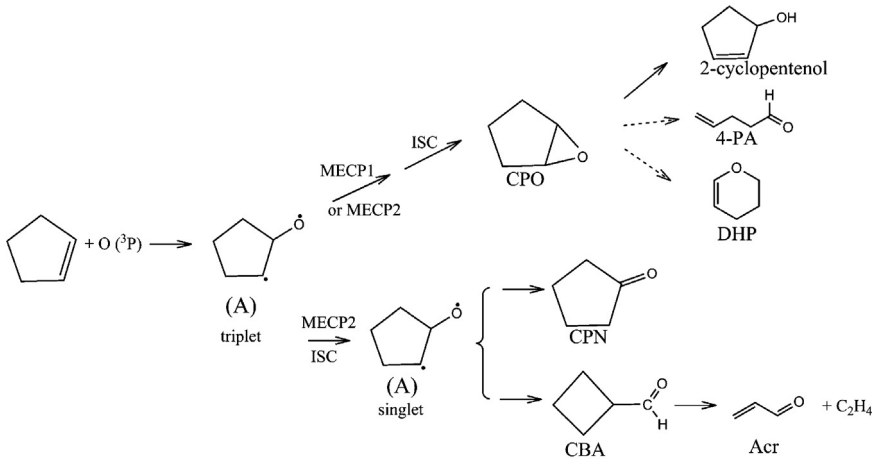

Scheme 2. Newly revealed nonadiabatic mechanism for the reaction $O(^3P) + c\text{-}C_5H_8$.

The energy of CBA (P6) (−82.9 kcal mol^{-1}) is almost as same as that of cyclopentenoxide (CPO) (P4) (−82.7 kcal mol^{-1}), while the decomposition barrier of CBA (P6) (^{1}TS4) is lower than all that of the rearrangement and decomposition pathways of cyclopentenoxide (CPO) (P4). Therefore it is expected that the product distribution of CBA (P6) should be smaller than that of cyclopentenoxide (CPO) (P4), if considering their secondary reactions.

3.4. The predicted product distribution and comparison with the experiments

Summarizing all the revealed adiabatic and nonadiabatic reaction pathways in Figs. 2 and 3, the product distributions can be predicted for the reaction of oxygen with cyclopentene. Energetically and kinetically, the major product should be P4, the cyclopentenoxide (CPO) because its formation is barrierless and requires the least reaction steps. The second major product should be P5, the cyclopentanone (CPN). Other important products are P6, the cyclobutylcarboxaldehyde (CBA) and its subsequent fragments of ethylene (C_2H_4) and acrolein (Acr) (P7). The secondary decomposition or rearrangement of the major product CPO also leads to some minor products, including P9 (4-PA), P10 (DHP), and P8 (cyclopentenol).

3.4.1. The major product

It can be seen from Fig. 3 that the addition of oxygen atom to cyclopentene leads to the formation of ^{3}IM1, and then it can cross to singlet state via MECP1 with a low barrier of only 0.2 kcal mol^{-1} and release CPO (P4) simultaneously. There is also another pathway to produce CPO (P4). The chair conformation ^{3}IM1 can rearrange to boat conformation ^{3}IM2 overcoming the barrier of 2.9 kcal mol^{-1}, and then cross to the singlet diradical ^{1}IM1 via MECP2. Starting from ^{1}IM1, CPO (P4) is formed directly, while CPN (P5) is formed via an H-shift transition state. Compared to cyclopentenoxide (CPO), the formation of cyclopentanone (CPN) obviously undergoes more steps and surmounts slightly higher barriers. Therefore, the product distribution of cyclopentenoxide (CPO) is expected to be larger than that of cyclopentanone (CPN). In the experiments of $O(^3P)$ and cyclopentene, both of cyclopentenoxide (CPO) and cyclopentanone (CPN) were observed to be the main products. Cvetanović et al. [13] found that the product yield of CPO (36.0%) was higher than that of cyclopentanone CPN (16.3%), while inverse product distribution was obtained in the experiment of Nothdurft et al. [14]. Our calculation supports the experimental results of Cvetanović et al. [13] that the cyclopentenoxide (CPO) is the major product.

3.4.2. Cyclopentenols predicted in our calculation

Carbonyl (keto) compounds are intermediates in the commonly accepted hydrocarbon oxidation mechanisms, while the enols, the less-stable isomer of carbonyl (keto), had not been included in standard models until 2005. Taatjes et al. [4] investigated the ethanol, propenols and butenols by photoionization mass spectrometry in hydrocarbon oxidation reaction and found that the yield of enols was significant. So they believed that normal hydrocarbon oxidation mechanisms should include the formation of previously unsuspected enols, which bear OH group adjacent to C=C double bond. To date, neither experimental nor theoretical research has involved the formation of cyclopentenols in the hydrocarbon oxidation reaction of $O(^3P)$ with $c\text{-}C_5H_8$. In this work, our calculation results show that 2-cyclopentenol (P8) could be an important product in the reaction.

From the potential energy profiles shown in Fig. 3, it can be seen that subsequent to the major product CPO (P4), four secondary products (P7–P10) can be yielded, among which the formation of 2-cyclopentenol (P8) channel is energetically more favorable than the other three. Both of the formation of P9 (4-PA) and P10 (DHP) requires overcoming higher barriers than that of P8 (cyclopentenol). It is thus expected that the product distribution of cyclopentenol should be larger than that of 4-pentenal (4-PA) and dihydropyran (DHP). Since 4-pentenal (4-PA) and dihydropyran (DHP) have been observed in previous experiments [13], the detection of the important new product, cyclopentenols, can be predicted to be feasible in future targeted experiments.

4. Conclusion

For the reaction of $O(^3P)$ with cyclopentene, the triplet and singlet potential energy surfaces are calculated at the CCSD(T)//MP2/6-311G(d,p) level and the minimum energy crossing points (MECP) between the two surfaces are located using the Newton–Lagrange method, from which the complex nonadiabatic reaction pathways are newly revealed. The most probable mechanism can be summarized in Scheme 2. The reaction is initiated by the addition of ground state oxygen atom to the double bond of cyclopentene yielding the initial adduct, a triplet diradical intermediate (A), where two MECPs exist in its proximity and result in intersystem crossing from triplet state to singlet state via low barriers of 0.2 kcal mol^{-1} (MECP1) and 2.0 kcal mol^{-1} (MECP2). Simultaneous to ISC, the most major primary product cyclopentenoxide (CPO) is directly formed by a barrierless ring closure process. The secondary rearrangement of CPO then leads to minor products of 2-cyclopentenol (P8), 4-PA (P9) and DHP (P10),

respectively. In parallel to the CPO formation, the intersystem crossing via MECP2 results in the singlet diradical intermediate (A), from which the second major product, cyclopentanone (CPN), is formed via a barrierless hydrogen shift, or another important product cyclobutylcarboxaldehyde (CBA) is produced with a low barrier of 4.1 kcal mol^{-1}. Careful IRC and spin density analysis shows here that the ring opening of the cyclic diradical intermediate (A) leads to the four-membered ring product CBA, instead of the previously proposed [13] acyclic diradical $C^{\bullet}H_2CH_2CH_2C^{\bullet}HCHO$. It is thus through the fragmentation of CBA to produce the secondary products of acrolein (Acr) and ethylene (C_2H_4). Overall, minimum energy crossing points (MECP) are found to play key roles resulting in the energetically favorable nonadiabatic reaction pathways.

The most probable reaction mechanism revealed here explains logically the experimentally observed product formation of CPO, CPN, CBA, acrolein + ethylene, 4-PA, and DHP, demonstrating further the origin of the rich chemistry of $O(^3P)$ with cyclopentene. The product distributions are rationalized, which clarifies previous controversy about whether CPO or CPN is the most major product. In addition, important new product of cyclopentenol, one of the unsuspected enol type of oxidation intermediates in hydrocarbon flames, is predicted here to be energetically accessible and could be possibly detected in the combustion of cyclopentene flames.

Acknowledgments

This work was financially supported by the National Natural Science Foundation of China (grant nos. 21203206 and 21333012) and the National Basic Research Program of China (2013CB834602).

References

[1] S. Roszak, R.J. Buenker, P.C. Hariharan, J. Kaufman, J. Chem. Phys. 147 (1990) 13.
[2] P. Casavecchia, G. Capozza, E. Segoloni, F. Leonori, N. Balucani, G.G. Volpi, J. Phys. Chem. A 109 (2005) 3527.
[3] F. Leonori, A. Occhiogrosso, N. Balucani, A. Bucci, R. Petrucci, P. Casavecchia, J. Phys. Chem. Lett. 3 (2012) 75.
[4] C.A. Taatjes, N. Hansen, A. McIlroy, J.A. Miller, J.P. Senosiain, S.J. Klippenstein, F. Qi, L. Sheng, Y. Zhang, T.A. Cool, J. Wang, P.R. Westmoreland, M.E. Law, T. Kasper, K. Kohse-Höinghaus, Science 308 (2005) 1887.
[5] D.J. Garton, T.K. Minton, W. Hu, G.C. Schatz, J. Phys. Chem. A 113 (2009) 4722.
[6] J.T. Paci, H.P. Upadhyaya, J. Zhang, G.C. Schatz, T.K. Minton, J. Phys. Chem. A 113 (2009) 4677.
[7] H.M. Su, S.L. Zhao, K.H. Liu, T.C. Xiang, J. Phys. Chem. A 111 (2007) 9600.
[8] J. Warnatz, U. Maas, R.W. Dibble, Combustion, Springer, Heidelberg, 1996.
[9] K. Hoyermann, F. Mauss, T. Zeuch, Phys. Chem. Chem. Phys. 6 (2004) 3824.
[10] J.M. Simmie, Prog. Energy Combust. Sci. 29 (6) (2003) 599.
[11] R.J. Cvetanović, J. Phys. Chem. Ref. Data 16 (1987) 261.
[12] R.J. Cvetanović, J. Phys. Chem. 74 (1970) 2730.
[13] R.J. Cvetanović, D.F. Ring, L.C. Doyle, J. Phys. Chem. 75 (1971) 3056.
[14] K. Hoyermann, J. Nothdurft, M. Olzmann, J. Wehmeyer, T. Zeuch, J. Phys. Chem. A 110 (2006) 3165.
[15] C. Moller, M.S. Plesset, Phys. Rev. 46 (1934) 618.
[16] C. Gonzalez, H.B. Schlegel, J. Phys. Chem. 94 (1990) 5523.
[17] J.A. Pople, M. Head-Gordon, K. Raghavachari, J. Chem. Phys. 87 (1987) 5968.
[18] N. Koga, K. Morokuma, Chem. Phys. Lett. 119 (1985) 371.
[19] H.M. Zhao, W.S. Bian, K. Liu, J. Phys. Chem. A 110 (2006) 7858.
[20] S.L. Zhao, W.Q. Wu, H.M. Zhao, H. Wang, C.F. Yang, K.H. Liu, H.M. Su, J. Phys. Chem. A 113 (2009) 23.
[21] M.J. Frisch, G.W. Trucks, H.B. Schlegel, G.E. Scuseria, M.A. Robb, J.R. Cheeseman, J.A. Montgomery Jr., T. Vreven, K.N. Kudin, J.C. Burant, J.M. Millam, S.S. Iyengar, J. Tomasi, V. Barone, B. Mennucci, M. Cossi, G. Scalmani, N. Rega, G.A. Petersson, H. Nakatsuji, M. Hada, M. Ehara, K. Toyota, R. Fukuda, J. Hasegawa, M. Ishida, T. Nakajima, Y. Honda, O. Kitao, H. Nakai, M. Klene, X. Li, J.E. Knox, H.P. Hratchian, J.B. Cross, V. Bakken, C. Adamo, J. Jaramillo, R. Gomperts, R.E. Stratmann, O. Yazyev, A.J. Austin, R. Cammi, C. Pomelli, J.W. Ochterski, P.Y. Ayala, K. Morokuma, G.A. Voth, P. Salvador, J.J. Dannenberg, V.G. Zakrzewski, S. Dapprich, A.D. Daniels, M.C. Strain, O. Farkas, D.K. Malick, A.D. Rabuck, K. Raghavachari, J.B. Foresman, J.V. Ortiz, Q. Cui, A.G. Baboul, S. Clifford, J. Cioslowski, B.B. Stefanov, G. Liu, A. Liashenko, P. Piskorz, I. Komaromi, R.L. Martin, D.J. Fox, T. Keith, M.A. Al Laham, C.Y. Peng, A. Nanayakkara, M. Challacombe, P.M.W. Gill, B. Johnson, W. Chen, M.W. Wong, C. Gonzalez, J.A. Pople, Gaussian, Inc., Wallingford, CT, 2004.
[22] M.D. Scheer, R. Klein, J. Phys. Chem. 73 (1969) 597.
[23] (a) S. Antolínez, J.C. López, J.L. Alonso, Angew. Chem. 111 (1999) 1889; (b) S. Antolínez, J.C. López, J.L. Alonso, Angew. Chem. Int. Ed. 38 (1999) 1772.
[24] S. Antolínez, A. Lesarri, J.C. López, J.L. Alonso, Chem. Eur. J. 6 (2000) 3345.
[25] J. Kraitchman, Am. J. Phys. 21 (1953) 17.